Volume 1 | Number 1 | Jan 2013 | Pages 1–100

Journal of
Materials Chemistry B

Materials for biology and medicine
www.rsc.org/materialsB

ROYAL SOCIETY OF CHEMISTRY

ROYAL SOCIETY OF CHEMISTRY

www.rsc.org/materialsB

Journal of Materials Chemistry B

ARTICLE

Small Bioactive Molecules as Dual Functional Co-dopants for Conducting Polymers

J. A. Goding[a], A. D. Gilmour [a], P.J. Martens [a], L. A. Poole-Warren [a] and R. A. Green [a]

Biological responses to neural interfacing electrodes can be modulated via biofunctionalisation of conducting polymer (CP) coatings. This study investigated the use of small bioactive molecules with anti-inflammatory properties. Specifically, anionic dexamethasone phosphate (DP) and valproic acid (VA) were used to dope the CP poly(ethylenedioxythiophene) (PEDOT). The impact of DP and VA on material properties was explored both individually and together as a codoped system, compared to the conventional dopant p-toluenesulfonate (pTS). Electrical properties of DP and VA doped PEDOT were reduced in comparison to PEDOT/pTS, however co-doping with both DP and VA was shown to significantly improve the electroactivity of PEDOT in comparison the individually doped coatings. Similarly, while the individually doped PEDOT coatings were mechanically friable, the inclusion of both dopants during electropolymerisation was shown to attenuate this response. In a whole-blood model of inflammation all DP and VA doped CPs retained their bioactivity, causing a significant reduction in levels of the pro-inflammatory cytokine TNF-α. These studies demonstrated that small charged bioactive molecules are able act as dopants for CPs and that co-doping with ions of varied size and doping affinity may provide a means of addressing the limitations of large bulky bimolecular dopants.

Introduction

Conducting polymers (CPs) have become a focal point of research into next-generation electrode materials due to their superior electrical properties for charge transfer in biological environments. Perhaps the greatest potential of CPs within neural applications is their ability to accommodate biofunctionality through the incorporation and controlled release of bioactive molecules. Incorporation of neurotrophic factors, cell adhesion molecules and various drug compounds within CPs has been shown to assist in the development of higher quality tissue-electrode interfaces[1–10]. However, limitations associated with the deterioration of mechanical and electrochemical properties of biofunctionalised CPs restrict their application to medical devices[6,7,11].

One method used to impart biofunctionality to CPs has been the use of bioactive dopants. While this has been shown to be effective in incorporating bioactive molecules which can be accessed by cells in the biological environment, it has been shown to result in degradation of the CP mechanical and electrochemical stability. Many of the bioactive molecules investigated as dopants in the literature have been large biological molecules, such as proteins and peptide fragments with molecular weights ranging from $1 - 23$ kDa[6,12]. It has been shown that these molecules typically result in significant reduction in CP coating cohesiveness, increasing friability and delamination[6,12].

Studies by Baek *et al* have demonstrated that larger dopant molecules produce films of greater stiffness, which may make them more prone to brittle failure[13]. This effect is due to the biomolecules interfering with and limiting the efficiency of the electrodepositon process[6,12,14]. It is possible that the use of smaller bioactive dopants will attenuate issues related to film cohesiveness as smaller molecules are less likely to interfere with the electrodeposition process. In this study two small drug compounds, dexamethasone phosphate (DP) and valproic acid (VA), are investigated as dopants for the conducting polymer poly(3,4-ethylenedioxythiophene) (PEDOT).

DP is an ionic form of dexamethasone, a glucocorticoid steroid and a powerful anti-inflammatory drug with a low molecular weight of 493 Da (see Figure 1). Dexamethasone has been shown to effectively reduce astroglial response and neuronal death in the tissue surrounding a neural implant[17,18]. There are several reports of the use of DP as a dopant in a variety of CPs. Wadhwa *et al* report the use of DP as a dopant for polypyrrole (PPy)[19]. Stevenson *et al* investigated the use of DP in polyterthiophene and characterised the resultant coatings active and passive drug release properties[20,21]. These studies were primarily concerned with the controlled release of DP from the electrode coatings. To date, no comparative studies have been made on the effect that DP has on the electrochemical and mechanical properties of CPs.
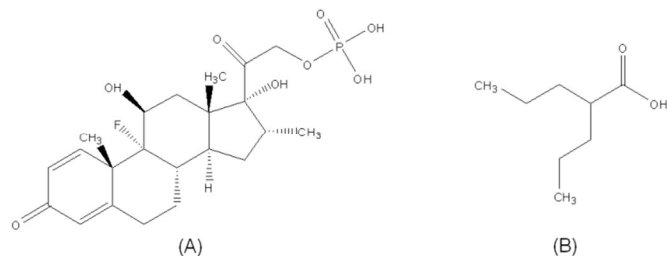
Figure 1 - Chemical structure of bioactive dopants: (A) Dexamethasone phosphate; (B) Valproic acid

Valproic acid (VA) is a branched, short chain hydrocarbon (fatty acid) which is conventionally used as an anticonvulsant for epilepsy and as a mood stabiliser for bipolar disorder. VA (shown in Figure 1) has a molecular weight of 144 Da[22]. However, there is growing evidence that VA also possesses a range neuroprotective and neuroregenerative properties[22–29].

Several *in vitro* studies have demonstrated the neuroprotective and neurogenic properties of VA. VA enhanced survival of rat retinal ganglion cells in culture by 63% compared to the untreated control[26]. Treating primary neurons from embryonic rat spinal cord with VA has been shown to increase the expression of brain-derived neurotrophic factor and encouraged neurite formation in the presence of Nogo-A peptide, an axonal growth inhibitor[29]. The neuroprotective and anti-inflammatory properties of VA have also been demonstrated in several *in vivo* studies investigating recovery in models of CNS damage such as spinal cord injury or stroke. A single injection of VA in an ischemia-reperfusion injury in rat cerebrum was found to supress both oxidative damage and microglial activation[23]. Administration of VA following spinal cord injury in rats resulted in significantly improved locomotor function and decreased presence of macrophages in the surrounding tissue[25]. To date there have been no reports on the use of VA in CPs.

Of particular interest is the effect of dual doping CPs with these bioactive dopants. Studies have shown that the use of dual dopants can result in improved electrochemical properties due to changes in molecular conformation in the CP backbone[30-34]. One approach to dual doping is *in-situ* co-doping, in which multiple dopants are supplied in the solution from which the CP is polymerised. Bhandari *et al* demonstrated a synergistic effect when polyaniline (PANI) was co-doped with sulphuric acid and p-toluenesulfonate[30]. It was determined that co-doping altered the charge density along the CP backbone in a concentration-dependent nature. At certain molar ratios, incorporation of dual dopants produced PANI films with better conduction than those obtained when using only a single dopant.

It has been suggested that dopant molecules with weaker hydration are capable of stronger interactions with CPs when in solution, making it easier to act as a counter-ion during the polymerisation process[35,36]. From this work, the following dopant series for CPs was identified from strongest to weakest counter-ion affinity:

$$S_2O_3^{-2} > Br^-, ClO_4^- > SO_3^- > Cl^-, COO^- > H_2PO_4^-, HPO_4^{-2}$$
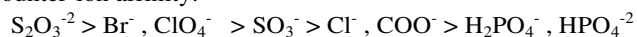
In this series the carboxyl anion (dopant group in VA) and the phosphate anion (dopant group in DP) are adjacent and hence share similar counter-ion affinity with PEDOT. Co-doping with these two bioactive dopants may not only help offset detrimental effects of biomolecules on electrochemical properties, but may also provide a biological synergistic effect which benefits from both the anti-inflammatory properties of DP as well as the neuroprotective and neurotrophic effects of VA. No studies to date have examined the effect of co-doping CPs, where both dopants are bioactive molecules.

The primary objective of this study was to gain an understanding of the use of two bioactive dopants, DP and VA within CPs. Specifically, the potential for co-doping PEDOT with both DP and VA was investigated and the resultant bioactive CP characterised through analyses relevant to performance in neuroprosthetic electrodes. The impact of VA and DP incorporation was assessed in comparison to p-toluenesulfonate (pTS), a conventional and well characterised CP dopant.

Experimental Methods

Electropolymerisation

Unless stated otherwise all reagents were obtained from SigmaAldrich. All PEDOT coatings were deposited from precursor solutions using a 1:1 mix of deionised (DI) water and acetonitrile as a solvent containing 100 mM EDOT. Single dopant PEDOT coatings were doped with 25 mM of either DP or VA. Co-doped PEDOT was doped with 12.5 mM of both DP and VA. Control coatings of PEDOT doped with 12.5 mM of pTS were produced under identical conditions. PEDOT coatings were galvanostatically electrodeposited onto platinum disc electrodes (0.5 cm^2 deposition area) using an eDAQ potentiostat at 6 mA.cm^{-2} for 3min and 45 sec versus a platinum counter electrode. This high current density was required to enable the formation of PEDOT/VA coatings, and was kept constant for all dopant types. Following deposition, each coating was washed three times in DI water to remove process contaminants. For all electrochemical and biological characterisations, PEDOT electrodes were compared to bare platinum electrodes as a conventional "gold standard" electrode material.

Scanning Electron Microscopy (SEM)

PEDOT coatings were imaged using a Hitachi S3400 SEM under high-vacuum with a 15kV probe potential at 2500 x magnification. Due to the conductive nature of the coatings no additional coatings were required for imaging.

X-ray Photoelectron Spectroscopy (XPS)

XPS analysis was conducted using a Thermo Scientific ESCALAB250Xi using a pass energy of 20eV. Curve fitting was performed (Eclipse Datasystem V2.1, USA) and where curves were found to contain more than one chemical state of a given species, the PeakFit function was used to elicit the

different chemical states. The intensity ratio of the doublet was maintained at 2:1 and the energy separation was maintained at 1.18 eV. Relevant spectral peaks (refer to Table 1) were used to confirm the incorporation of dopants and to determine the relative doping ratio. The doping ratio is defined as the ratio of peak integral of the dopant signal (S2p3-C, P2p-A, C1s-C) to the peak integral of the PEDOT signal (S2p3-A + S2p3-B). For the PEDOT/(DP+VA) coating the P2p-A peak was used to determine the amount of DP present. This amount was then subtracted from the C1s-C signal, which captures both DP and VA, to calculate the amount of VA present. Data was obtained from three independent samples for each variant.

Table 1 - Identification of characteristic XPS peaks and their associated chemical species.

Bond Orbital	Peak Location (eV)	Bond Structure	Chemical Species
S2p3-A	164	C-S-C	PEDOT
S2p3-B	165	C-S-C	PEDOT
S2p3-C	168	$-SO_3^-$	pTS
P2p-A	134	$-PO_3^{2-}$	DP
C1s-C	288	$-C=O$	VA, DP

Cyclic Voltammetry (CV)

In order to evaluate the impact of using DP and VA as dopants in PEDOT electrodes, CV and EIS were conducted to examine the charge transfer characteristics and electrochemical stability of these coatings. The charge storage capacity (CSC) and electrochemical stability of PEDOT coatings was determined using an eDAQ potentiostat and e-corder unit coupled with the supplied EChem software package. Samples were scanned in 0.9% saline solution between -0.8 V and 0.6 V versus an isolated Ag/AgCl reference electrode at a scan rate of 150 mV.s^{-1} for 800 continuous cycles. CSC was calculated by integrating the current response with respect to time. Electrochemical stability was calculated as the change in CSC over the 800 CV cycles. Scans were conducted on six independent samples for each electrode composition.

Electrochemical Impedance Spectroscopy (EIS)

The frequency dependant charge transfer characteristics of bioactive PEDOT coatings were examined through EIS. EIS was conducted using an eDAQ electrochemical impedance analyser and potentiostat coupled with the supplied Z100 Navigator software package. Samples were scanned using a 100 mV AC signal across a frequency range of 10^4 to 10^{-1} Hz. Results were presented as Bode plots with both the impedance and phase angle analysed. Scans were conducted on five independent samples for each electrode composition.

Film Delamination

To evaluate the impact of the bioactive dopants on the mechanical cohesiveness of PEDOT coatings, delamination was tested using a modified ASTM tape adhesion test (D3359-02). This test involves deliberately causing damage to a film and then applying an adherent force (tape) to determine coating adhesion and friability[6,11,37]. An X-cut was made in the PEDOT

coating using a scalpel blade before applying standard Scotch 3M "low-medium adhesion masking tape for delicate surfaces" (#2080) to the surface of the PEDOT coating. The tape was allowed to sit for 5 min, after which it was slowly peeled back off the electrode surface maintaining a 180° angle between the tape and the electrode surface. A Leica M80 stereoscope was used to image the PEDOT coatings before and after delamination. Images of the PEDOT coatings were analysed by converting first to greyscale and then to a binary black and white image to differentiate the intact coating from exposed platinum substrate. Extent of delamination was determined by the shift from black (CP coating) to white (underlying platinum). Tests were conducted on five independent samples for each dopant variant.

TNF-α Assay

The anti-inflammatory properties of bioactive PEDOT coatings were assessed through measurement of TNF-α, a pro-inflammatory cytokine, following exposure of CPs to whole blood. Blood was collected from healthy human donors (Human Research Ethics Committee No. 14108; The University of New South Wales) into 10 mL vacutainers containing 158 USP units of sodium heparin (Becton Dickinson and Company). PEDOT and platinum samples were disinfected using a 90 minute exposure of both the top and bottom faces of the samples to UV light inside a laminar flow hood (Email Air Handling). Samples were placed in 24-well plate and 980 µL of blood was added to each well. Positive control samples and relevant experimental samples were stimulated with 20 µL of a 250 µg.mL-1 solution of lipopolysaccharide (LPS) in Dulbecco's phosphate buffered saline (DPBS) in order to trigger a known inflammatory response. Negative controls (blood with no sample) and all remaining experimental samples were dosed with 20 µL of DPBS vehicle.

Samples were incubated for 1 hour at 37°C in a 5% CO_2 humidified atmosphere. Blood was collected from the well plates and centrifuged at 1600 RPM for 15 minutes. Blood plasma was collected and stored at -80°C before quantification by ELISA. Plasma samples were assayed using a Quantikine Human TNF-α ELISA kit (R&D Systems). The concentration of TNF-α was quantified by measuring the optical density at 490nm compared to baseline measurements made at 570nm. The fluorescence values were quantified by matching to a standard curve obtained from known solutions of TNF-α. Measurements were made for three samples of each electrode composition for each study replicate, with a total of three replicates. Statistical analysis of TNF-α concentration was conducted using a one-way ANOVA with Sidak multiple comparisons

Astrocyte-enriched Glial Culture

The response of primary glial cells cultured on PEDOT electrodes was used as a model to assess the immune response of CNS tissue to bioactive PEDOT coatings. A mixed primary culture of astrocytes and microglia was extracted from P1 neonatal mice (Swiss Taconic) in accordance with University of

New South Wales animal ethics protocols (ACEC 13/44A). Extraction and isolation of cells was based on the methodology outlined by McCarthy and De Vellis[38]. Briefly, the forebrain was explanted and the meninges removed prior to dissection of the cerebral cortices. The cortices were placed in HBSS (-Mg^{2+}, -Ca^{2+}) and the tissue was dissociated with a 3mL glass pasture pipette. The tissue was then digested using two 20 minute pulses in the presence of trypsin EDTA (0.25%) and collagenase (0.1 mM). Trypsin was deactivated using a stop digestion mix (soybean trypsin inhibitor and DNase). Cells were allowed to settle out of suspension before decanting excess media. Cells were triturated using three passes through a 21 gauge needle followed by two passes through a 23 gauge needle. Cells were transferred to a 15 ml tube and 3 mL of fresh media (DMEM + 4.5 g.L-1 glucose + 10% FBS + 1% penicillin streptomycin) was added before being centrifuged for 5 minutes at 1200 RCF. The supernatant was decanted and replaced with 5 mL of fresh media before resuspending cells using a 3 mL glass pasture pipette in a T75 tissue culture flask (PLL coated using 15 minute incubation in 134 µg.mL-1 solution in DI water).

Prior to plating, all samples were placed in 24 well plates and disinfected by soaking in 80% ethanol for 1 hour. Following disinfection, samples were washed three times in DPBS and coated with PLL by incubation for 15 minutes in 0.5 mL of PLL solution (134 µg.mL-1 PLL in cell culture water). The coating was rinsed three times with DI water and left to dry overnight. To plate the astrocyte enriched culture, the cell culture media was removed from the T75 tissue culture flask and the flask was rinsed twice with 5 mL of DPBS. Cells were trypsinised in a 0.25% solution for five minutes. The solution was transferred to 15 mL tube and centrifuged at 1200 RPM for 5 minutes. The supernatant was decanted and the cell pellet resuspended in 1 mL of media. The cell concentration was determined using a haemocytometer and adjusted to a concentration of 80,000 cells.mL^{-1}. Cells were plated on samples, in 24 well plates, at a density of 40,000 cells per well (0.5mL per well equating to 23,000 cells.cm^{-1}). Culture media was renewed every 48-72 hours with total exchange of 0.5 mL of media. Four images were captured at random locations on each sample, with three replicate samples in each of the two experimental repeats.

Glial cell response was characterised by cell morphology and size as well as expression and structure of GFAP. When an astrocyte shifts away from a fibrous morphology and towards a hypertrophied, protoplasmic morphology, it increases in size and upregulates expression of GFAP, which are clear indicators of astrocytes becoming reactive[39,40]. A secondary indicator of severe reactive astrocytosis is the loss of distinct cellular domains[41]. These processes reflect the *in vivo* process of astrocyte activation and formation of a glial scar[18,42]. Astrocyte morphology profiles were generated using a 5-point grading scale ranging from non-reactive fibrous astrocytes (A) to reactive protoplasmic astrocytes (E). Images were analysed by applying a threshold filter to the GFAP channel (ImageJ). The total cell coverage was defined as the percentage area of the image stained positive for GFAP. Cell morphologies were ranked by abundance for each image from most abundant (5) to least abundant (1). A score of zero was given if a particular morphology was not present. The average ranked abundance for each morphology grading was multiplied by the total cell coverage to estimate the ranked cell coverage (i.e. the approximate area of a sample covered by each type of astrocyte morphology).

Results and Discussion

Physicochemical Properties

CP coatings were successfully electrochemically deposited from all four precursor solutions. All PEDOT coatings were coherent, with the exception of PEDOT/VA which produced a sparser and non-uniform coating, revealing some of the underlying platinum substrate.

Scanning electron micrographs of PEDOT coatings doped with pTS, DP, VA and DP+VA are shown in Figure 2. It can be seen that the use of pTS as a dopant results in the highly nodular surface morphology characteristic of electrochemically deposited CP[13,43,44]. The use of the bioactive dopants, DP and VA, resulted in a substantial reduction in the roughness and nodularity of the PEDOT coatings with the reduction in nodularity being most pronounced in PEDOT/VA coatings. Additionally, the secondary nodular structure (micronodules on nodules) seen in PEDOT/pTS was supressed in the coatings containing DP and/or VA as a dopant. The morphology of the codoped PEDOT/(DP+VA) was closer to that of PEDOT/DP than PEDOT/VA, exhibiting the same reduction in nodularity compared to PEDOT/pTS. The suppression of the characteristic nodular texture is associated with a considerable reduction in surface area.

The formation of altered surface morphologies is due to differences in the size, charge density, nucleophilicity and steric effects of the dopant molecules used[13,30,45]. These factors all play a role in determining the efficiency of any specific dopant. While DP is considered small for a biological dopant and is significantly smaller than many biological dopants reported in the literature, it may be considered large when compared to pTS (493 Da vs. 155 Da respectively). In addition, it is likely to encounter significant steric hindrance due to its structure within a PEDOT network[6,46].

The phosphate group in DP is more electronegative and less nucleophilic than the sulfonate group in pTS meaning it is less willing to donate (or "less likely to dope") an electron to the π-bond in the PEDOT backbone. VA isn't likely to experience any significant steric hindrance, however, it is a very weak acid (pKa 4.6 compared to 1.9 for DP and -2.8 for pTS) and hence will only partially dissociate creating the potential for a deficit of free anions during electrodeposition[47]. Furthermore, the fraction of VA that is dissociated is even less nucleophilic than DP and as such, VA is expected to behave poorly as a dopant.
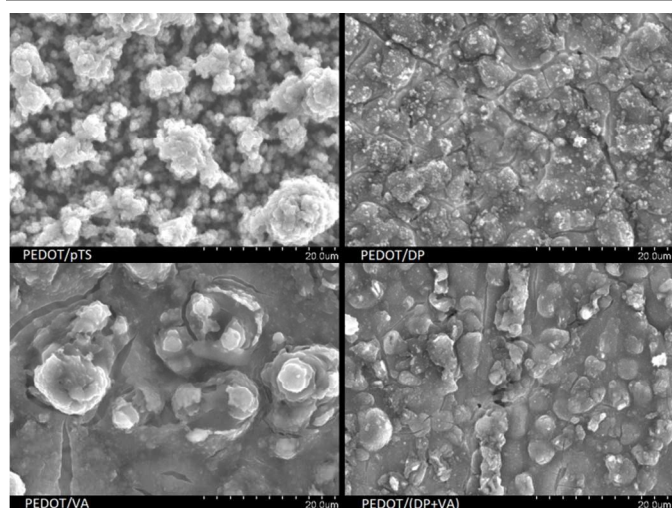
Figure 2 – SEM micrographs of PEDOT coatings doped with (clockwise from top left) pTS, DP, DP+VA and VA taken at 2,500X magnification.

A summary of the doping ratios as determined by XPS is presented in Table 2. Due to sample incompatibility with ion etching, XPS was restricted to surface only characterisation. As such the calculated doping ratios are from the top 10-20 atomic layers of the surface (approx. 20 nm). However, the doping level of conducting polymers does not change significantly with thickness after the initial transition from two-dimensional to three-dimensional growth[81]. The doping ratios of all PEDOT films fall within the typical range of $0.2 – 0.4$[12,48]. Incorporation of both DP and VA within PEDOT/(DP+VA) was confirmed. The use of pTS as a dopant provided the most reliable electrodepositions, whereas larger variation was observed when using DP and/or VA as dopants. The increase in variation of doping ratios for PEDOT films containing DP and/or VA may be symptomatic of poor dopant efficiencies.

Table 2 - Doping ratio of PEDOT films with varied dopant chemistry (n=3).

Composition		Doping Ratio	
		Avg	StDev
PEDOT/pTS		0.33	±0.03
PEDOT/DP		0.28	±0.13
PEDOT/VA		0.38	±0.18
PEDOT/(DP+VA)	DP	0.08	±0.02
	VA	0.26	±0.20
	VA+DP	0.34	±0.22

The inability of PEDOT/VA to form a coherent coating is another symptom of poor dopant efficacy. Furthermore, unlike other pre-cursor solutions which tend towards a brown-tinge post-deposition, the PEDOT/VA solution tended towards a translucent-to-opaque dark-blue solution. The dark-blue colour is characteristic of doped PEDOT and is believed to be imparted by PEDOT/VA oligomers in a liquid suspension[12]. This implies that VA is capable of doping PEDOT oligomers but that there is some mechanism preventing the cross-linking and network growth required to efficiently produce longer

PEDOT chains and subsequently, a conformal electrode coating. Similar observations of dark-blue, post-deposition solutions have been made by Green et al in PEDOT doped with short (10-12 amino acids) laminin fragments[6,12], and Collier et al who reported poor deposition efficiency in polypyrrole (PPy) doped with hyaluronic acid[14]. In both instances, it was suggested that incorporation of the dopant, and its associated oligomer, was being inhibited due to mass-transport limitations and steric hindrance. Mass-transport limitations are unlikely for VA due to its small size, however the effect of its poor doping efficiency on the deposition of PEDOT may be similar to the issues experienced when mass-transport limitations have been observed. That is, poor dopant efficiency may result in similar inhibition of polymerisation as occurs with poor dopant availability.

Electrochemical Properties

Figure 3 graphs the differences in CSC of all PEDOT films pre and post-CV. The use of bioactive dopants, DP and VA, resulted in a significant decrease in CSC, both initially and over repeated cycling, when compared to the conventionally doped PEDOT/pTS. This decrease in initial CSC is largely attributed to the decrease in nodularity, and hence surface area, of the bioactive PEDOT coatings. However, all PEDOT coatings still provide considerable benefit over bare platinum electrodes. Comparing the three bioactive PEDOT films it can be seen that the co-doped system had the highest CSC, approximately double that of PEDOT/VA.
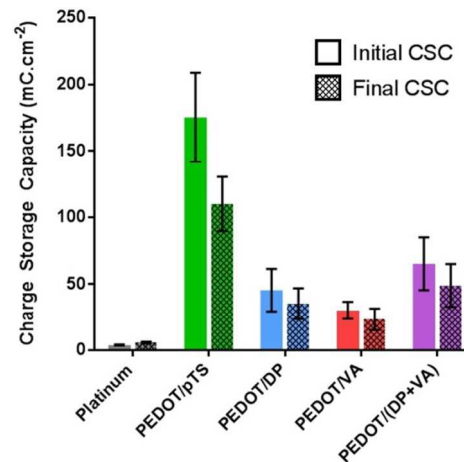

Figure 3 – Initial and final CSC of PEDOT coatings over 800 CV cycles. Error bars represent one SD from the mean (n=6).

A summary of the electrostability of PEDOT electrodes is provided in Table 3. All PEDOT coatings retained between 65 and 80% of their original CSC over 800 CV cycles, which is typical of electrodeposited PEDOT[11,49,50]. While the use of DP and/or VA as a dopant did decrease the absolute CSC of the PEDOT coatings, it did not negatively affect the electrostability of the coatings. The increase in CSC observed for bare platinum electrodes is due to the surface passivation of platinum[51].

Table 3 – Electrostability of bioactive PEDOT coatings after 800 CV cycles. Error values represent one SD from the mean (n=6).

Sample	Retained CSC (%)
Platinum	146.9 ± 8.7
PEDOT/pTS	64.1 ± 13.0
PEDOT/DP	78.3 ± 6.6
PEDOT/VA	76.6 ± 12.8
PEDOT/DP+VA	69.1 ± 16.8

The impedance magnitude and phase angle of all PEDOT coatings and bare platinum electrodes are represented in a bode plot in Figure 4. Of particular interest is the 1 - 500 Hz range as these are the frequencies in which neuroprosthetic electrodes typically record and stimulate[52,53]. It is also within this range that the PEDOT coatings offer the greatest advantage over bare platinum electrodes. Electrochemical impedance of electrodes within this frequency range where chemical reactions do not have time to progress, is largely determined by their surface roughness as capacitive charging dominates charge transfer mechanisms[52,54]. This phenomenon was reflected in the data where the impedance of the electrodes with low surface nodularity exhibited higher impedance magnitude and greater phase lag.
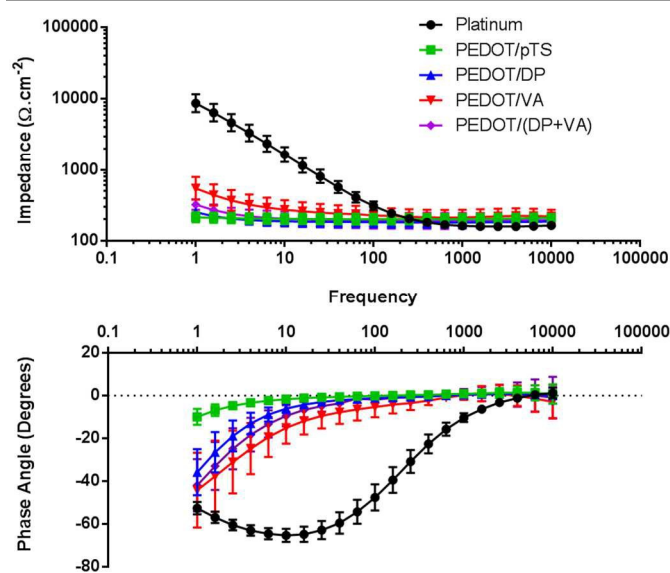

Figure 4 - Bode plot of impedance magnitude (top) and phase angle (bottom) of PEDOT coatings. Error bars represent one standard deviation from the mean (n=5).

All PEDOT coatings were found to have lower impedance magnitude and smaller phase angle compared to bare platinum at frequencies less than 100 Hz. At frequencies above 100Hz, where charge transfer shifts from non-faradaic to faradic modes, there was no significant difference in impedance between PEDOT and platinum electrodes. The PEDOT/pTS control coating was found to have an impedance of 215 Ω.cm^{-2} and -10° at 1 Hz. The use of DP and VA as dopants resulted in

relatively small, non-significant increases in impedance magnitude (253 Ω.cm^{-2} and 546 Ω.cm^{-2} respectively) and phase angle (-36° and -44° respectively) however again provided a significant improvement over bare platinum electrodes (8.72 kΩ.cm^{-2} and -53°). The co-doped PEDOT/(DP+VA) had an impedance of 324 Ω.cm^{-2} and -42° at 1 Hz. The codoping did produce a film with improved impedance in comparison to VA doped PEDOT at low frequency, but no significant or synergistic benefit was observed. This is thought to be due to the fact that charge transfer mechanisms are largely based on surface properties (particularly surface area) of the coatings and unlike CSC are not affected by the conformational changes in the PEDOT network caused by codoping.

Film Delamination

Representative images and a numerical summary of adhesion testing results are presented in Figures 5 and 6 respectively. All coatings, with the exception of PEDOT/VA, had minimal pre-delamination WPC (under 5%). PEDOT/VA had an initial WPC of 48% due to the non-conformal nature of the coating and the presence of cracks/flaws in the electrode coating as a result of VA's poor dopant efficiency. The PEDOT/pTS control experienced very little bulk film delamination (4.5% WPC), indicative of good coating adherence, concurring with prior studies[6,11]. In contrast the removal of coating experienced by the bioactive PEDOT variants (34%, 69% and 29% post-delamination WPC for PEDOT/DP, PEDOT/VA and PEDOT/(DP+VA) respectively) was severe enough to reveal the underlying platinum substrate. It should be noted that the removal of PEDOT occurred across the entire surface of the coating as opposed to being concentrated at the x-cut in the coating. This indicates that the mechanical failure is occurring within the coating (i.e. between polymer strands) not just between the PEDOT and the underlying platinum substrate, as is typical in delamination failures.
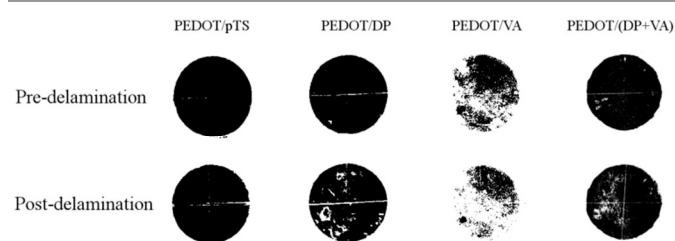

Figure 5 – Representative threshold images of PEDOT coatings pre-delamination coatings (top), and post delamination (bottom). The white areas indicate where PEDOT coating totally delaminated revealing underlying platinum substrate.

It should also be noted that PEDOT/pTS is considered mechanically robust within the CP class of materials. This assumption has been verified in the literature using the ASTM tape adhesion test to examine the delamination of both PEDOT and PPy using either pTS or poly(styrenesulfonate) (PSS) as a dopant[11]. PEDOT/pTS performed the best, losing only 0.5% of its coating, whereas PPy/PSS lost 51.1% of its coating.
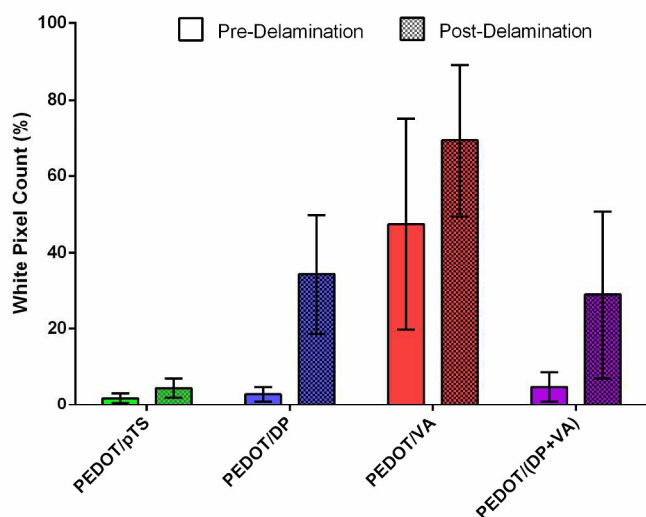
Figure 6 - Delamination of PEDOT coatings in ASTM x-cut assay. White pixel count is a relative measure of exposed, underlying platinum. Error bars are representative of one standard deviation from the mean (n=5).

In a separate study on PEDOT stability during sterilisation and accelerated aging, PEDOT/pTS was found to be the most stable PEDOT variant (compared to PSS and LiClO$_4$ dopants)[43]. Autoclave sterilisation and simulated aging (to an equivalence of two years of implantation) revealed delamination in all PEDOT coatings except PEDOT/pTS. Taking this into consideration, the mechanical robustness of PEDOT/DP and PEDOT/(DP+VA) is in line with other conventional CP systems. However, from an application perspective such a tendency to disintegrate and/or delaminate raises serious doubt over the expected lifetime of the coating in the context of chronically implanted devices which are expected to have service lifetimes of up to 70 years[55]. Studies examining the *in vivo* performance of PEDOT coated electrodes have noted mechanical delamination as a potential cause of increased impedance and access resistance for biphasic stimulation[56]. Other studies have noted the risk of mechanical delamination upon insertion of electrode shank probes[57]. It should be noted that the failure of the electrode coating will not cause critical failure of a device because the underlying metal electrode substrate will remain intact[58]. It will, however, mean the device could be limited to the charge transfer characteristics of the metal electrode. Ultimately this means that device design, in terms of safe charge delivery and electrode size will still be determined by the properties of the underlying metal electrode, not the CP.

Effect of co-doping PEDOT

One of the key aims of this study was to understand the effects of co-doping PEDOT with two bioactive molecules of different size and doping affinity. XPS confirmed incorporation of both DP and VA within PEDOT/(DP+VA) with doping ratios of 0.09 and 0.19 respectively. While it was expected that DP would be preferentially used as a dopant, it was observed that

VA was present in greater quantities. This could be a result of the increased mobility of VA in solution, compared to the more bulky DP, thus making it more available during electrodepositon. It should also be noted that XPS confirms the presence of the molecule within the CP network regardless of the molecule being incorporated as a dopant or merely as an entrapped molecule. Of the two other bioactive PEDOT systems assessed, the PEDOT/(DP+VA) was more similar to PEDOT/DP in terms of morphology as well as electrochemical and mechanical behaviour (see Figures 5 and 6). As such, DP is considered to be the dominant anion within the PEDOT/(DP+VA) system. One way of considering the co-doped system is that of PEDOT/DP wherein half of the DP has been replaced with VA. From this viewpoint, you might expect this would be accompanied by a decrease in CSC due to the poor doping efficiency of VA, however, the opposite is observed with PEDOT/(DP+VA) having the highest CSC of the bioactive PEDOT variants. One possible explanation for this is that VA acts as a "bridging" dopant when DP is not available due to transport limitations (which were exaggerated due to the high charge density of deposition). In the films where only DP was used as a dopant it is likely that the local deficiency of available dopant anions would result in overoxidation and/or structural defects in the growing PEDOT network. As discussed above, there is evidence that VA might be sufficient as a dopant for shorter chain oligomers but not for longer polymer chains. In the context of the co-doped system, this would mean that VA bridging prevents the formation of defects due to local DP deficiencies without encountering the same chain-growth inhibition observed in the PEDOT/VA system. This concept is illustrated in Figure 7.
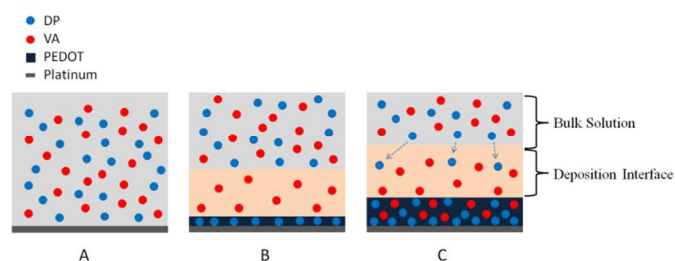

Figure 7 – VA bridging due to mass transport limitations

Figure 7A shows the system at equilibrium before the initiation of electrochemical deposition. Once deposition is initiated (Figure 7B), PEDOT will deposit onto the platinum substrate (monomer not shown in solution for the sake of clarity) preferentially using DP as a dopant. This leads to the formation of a mass transport-limited zone at the deposition interface. As the deposition progresses (Figure 7C), DP will diffuse from the bulk solution into the deposition interface. DP will still be preferentially used as a dopant, however DP incorporation will be limited by the rate at which it is diffusing into the interface resulting in the uptake of VA as dopant when DP is not locally available.

An alternative theory to explain the increase in CSC for co-doped systems, as suggested by Bhandari *et al*[30], is that incorporation of dual dopants establishes variations in charge density and counter ion distribution along the CP backbone thus facilitating increased intermolecular charge transport. Intermolecular charge transport (charge hopping) is highly dependent upon the physical arrangement of CP chains, particularly the intermolecular separation and orientation[59,60]. It is possible that the variation in charge density that arises from co-doping results in a more favourable packing of PEDOT chains thus resulting in increased charge mobility. Regardless of the underlying mechanism, the use of dual dopants may be an effective means to minimise the negative impact that bioactive dopants have on the electrochemical properties of CPs.

Biological Properties

Figure 8 shows the concentration of TNF-α in plasma after samples were incubated in whole blood for 1 hour. It can be seen that none of the PEDOT samples generated a significant upregulation of TNF-α. The positive control stimulated with LPS (5 µg.mL-1) generated significantly higher levels of TNF-α as expected. Statistical analyses showed a significant reduction in TNF-α for both DP containing films compared to the negative control (unstimulated blood). No significant reduction was observed for PEDOT/VA. This result demonstrates that no inherent inflammatory reaction was caused by exposure to any the PEDOT coatings. Furthermore, PEDOT containing DP was capable of reducing the inflammatory response below that of the negative control with PEDOT/DP and PEDOT(DP+VA) having TNF-α levels of 70 and 63 pg.mL-1 respectively compared to 160 pg.mL-1 for the negative control.

Figure 9 shows the results of a challenge study in which all samples were actively stimulated with LPS (5µg.mL-1) to generate a positive inflammatory response. It was observed that all three bioactive PEDOT coatings were capable of significant attenuation of the stimulated inflammatory response, however, no significant difference was observed between bioactive PEDOT coatings. Synergistic biological behaviour was not observed between DP and VA in the co-doped PEDOT. However, results demonstrate that both the incorporated DP and VA retain their bioactivity and are capable of significant attenuation of inflammatory responses within the one hour time frame of passive release (release via passive diffusion as opposed to active release via electrical stimulation of the PEDOT coating). These findings are in accordance with those of Wadhwa *et al* who found that incorporated DP, actively released from PPy retained its bioactivity and was capable of reducing inflammatory reactions[19].

The lack of synergistic effect between DP and VA can be explained by looking at their respective mechanisms of action. The anti-inflammatory properties of DP are the result of up-regulation of anti-inflammatory factors and down-regulation of pro-inflammatory factors, effectively preventing the recruitment of leukocytes[15,16]. The anti-inflammatory mechanism initiated by VA is the result of its inhibition of histone deacetylases which regulates transcriptional activity of chromatin[22]. The resulting modification of gene expression down-regulates pro-inflammatory factors preventing the formation of reactive oxygen species (suppression of nitric oxide synthase) and suppressing neutrophil recruitment[22,23]. Although the mechanism of modulating gene expression differs between DP & VA, both act to supress the expression of TNF-α thus inhibiting activation of leukocytes[61,62]. This is a significant overlap in biochemical pathways, and as such it is not surprising that no synergistic effects between DP and VA were observed within this model.
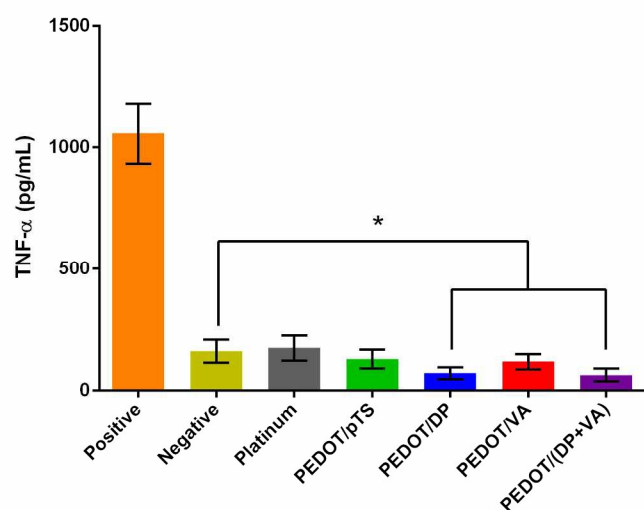

Figure 8 - Concentration of TNF-α in human plasma after 1 hour incubation in whole blood without LPS stimulation. Error bars represent one standard deviation from the mean (n=3, p<0.05).
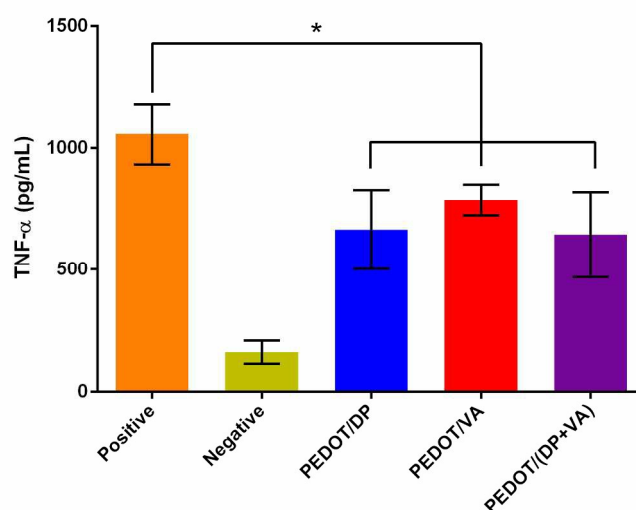

Figure 9 - Concentration of TNF-α in human plasma after 1 hour incubation in whole blood with LPS stimulation. Error bars represent one standard deviation from the mean (n=3, p<0.05).

Studies examining the response of primary glial cells in culture to PEDOT coatings suggested that there was no inhibition of cell growth in contact with any of the materials tested. A series of representative images of astrocytes after 14 days *in vitro* are shown in Figure 10. Astrocytes cultured on glass have a regular size with fine fibrous GFAP filaments, indicating they are generally non-reactive. Astrocytes cultured on platinum have mixed morphologies with a trend towards increased GFAP and hypertrophy (increased cell body size) indicating mild gliosis. Astrocytes cultured on PEDOT/pTS exhibited moderate hypertrophy and GFAP upregulation combined with the loss of clearly defined cell domains, indicating moderate gliosis. Astrocytes cultured on the bioactive PEDOT coatings exhibited significant hypertrophy and GFAP upregulation but retained clearly defined cellular domains indicating moderate gliosis. The basal layer of astrocytes directly in contact with the PEDOT coatings formed densely packed layers. Astrocytes on top of this dense basal layer retained more regular sizes and morphologies similar to those seen on glass, suggesting that the physical structure of the PEDOT coatings acts as a chronic irritant to the basal layer of astrocytes. The stratified structure was more prominent in the bioactive PEDOT coatings compared to PEDOT/pTS, this may be due to the difference in surface morphology and roughness.
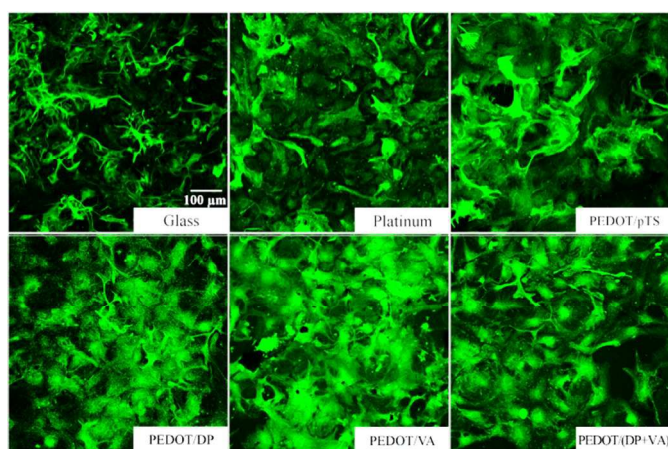

Figure 10 - Representative images of primary astrocyte morphology after 14 days *in vitro*. Green stain showing GFAP structure expressed by astrocytes.

Figure 11 shows the morphology profiles of astrocytes cultures as a function of ranked cell coverage (i.e. the approximate area of a sample covered by each type of astrocyte morphology). It was clear that total cell coverage on the control materials was significantly higher than that of the CP coated platinum. Analysis of the area of GFAP fluorescence showed that glass and platinum experienced very similar cell coverage, being 87 +/- 5% and 85 +/- 4% respectively. All PEDOT variants had analogous average cell coverage, but the bioactive variants presented with greater variability in results. Specifically, the PEDOT/VA experienced the highest variability with average cell coverage and standard deviation of 56 +/- 24%. The DP doped PEDOT was comparable to the control PEDOT/pTS with these materials having 56 +/- 6% and 56 +/- 9% of cell

coverage, respectively. Finally, the dual doped PEDOT/DP+VA was observed to have a 57 +/- 12% cell coverage. These results again suggest that the interaction of the astrocytes with the underlying material is dominated by the material surface morphology, with the rough CP surface impacting on both cell attachment and functional reaction.
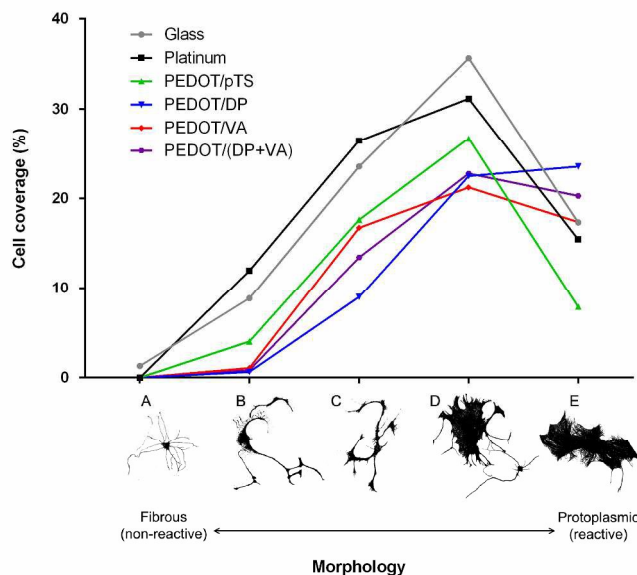

Figure 11 – Morphology profiles of astrocyte cultures as a function of cell coverage area (n=2). Astrocytes morphology was graded on a 5-point scale from non-reactive fibrous astrocytes (A) to reactive protoplasmic astrocytes (E).

For cultures on glass, platinum and PEDOT/pTS D-type morphologies (shown on x-axis of Figure 11) were the most abundant. Cultures on bioactive PEDOT coatings saw an increase in E-type morphologies, indicating a shift towards greater glial activation. There was some indication that incorporation of VA resulted in a shift towards fibrous morphologies of astrocytes in comparison to other bioactive PEDOTs assessed. An increase in the number of C-type morphologies were observed for coatings containing VA compared to PEDOT/DP, however further investigation of astrocyte function through biochemical assays are required.

Peng *et al* observed that protracted pre-treatment of primary neuron-glia co-cultures (rat midbrain) with VA reduced LPS-induced release of pro-inflammatory factors such as TNF-α, nitric oxide and intracellular reactive oxygen species by suppressing glial activation and decreasing the number of microglia[61]. This treatment had the effect of protecting neurons from LPS-induced cytotoxicity. The effect of VA was found to be concentration dependent, with a pre-treatment concentration of 0.6 mM resulting in complete restoration of neuron function following LPS stimulation. In an *in vivo* model of cerebral ischemia in rats, regular post-treatment with VA (300 mg/kg dose every 12 hours for 7 days) was found to significantly suppress the activation of microglia but not astrocytes[63]. Again, treatment with VA reduced the concentration of pro-inflammatory markers acting to attenuate ischemia-induced

neuronal death and deficiency. From these literature reports, there are several explanations for the lack of observed anti-inflammatory action of VA in this study. The lack of biochemical assays probing inflammatory markers means relying solely on cellular morphology to infer cellular function. This method is less sensitive and robust and hence will result in greater difficulty in detecting any effects. Biochemical assays would significantly bolster observations and allow cellular morphology to be ascertained in combination with specific intracellular mechanisms. Furthermore, VA has been reported to primarily exert its therapeutic action on microglia, not astrocytes. The astrocyte-enriched nature of this culture may mean that the therapeutic effect of VA is overridden by the artificially exaggerated presence of activated astrocytes. Finally, regular treatment (or protracted pre-treatment) with VA was required in order to obtain a therapeutic effect. It is likely that insufficient amounts of VA were released from the PEDOT coatings to cause a significant effect over 14 days in culture. Active electrical stimulation of PEDOT coatings could be used to drive out a larger percent of the incorporated VA, however it is possible that the total amount of incorporated VA is insufficient to have a chronic therapeutic effect.

There was no indication of DP having a therapeutic effect at 14 days *in vitro*. DP is known to reduce activation of astrocytes and cause down-regulation of pro-inflammatory factors[15]. It is also known from the blood contact study that the DP incorporated within PEDOT is still biologically active post-fabrication. Therefore, it is likely that the amounts of DP released under passive diffusion were insufficient to have a therapeutic effect which was maintained over 14 days. In prior studies DP has found to be effective in reducing inflammatory response in tissue at concentrations of $0.2 - 0.7$ μM[64]. Wadhwa et al cultured primary mixed glial cells in media conditioned with 1 μM DP which had been actively released from PPy coatings and observed significant reduction in activation of astrocytes and microglia over a 3 day period[19]. However, cells were cultured on glass, not directly in contact with the PPy coating meaning that this study only investigated the effectiveness of released DP over an acute timeframe and not the glial response to the PPy coating. In similar studies exploring DP coated neural probes, Zhong and Bellamkonda observed significant attenuation of inflammatory response at 1 and 4 weeks post-implantation from an estimated DP release concentration of 0.36 μM[18]. Without examining the release potential of the bioactive PEDOT coatings in this study, it isn't possible to make an estimate of the local concentrations of released DP and VA. However, it is unlikely that the amounts released from passive diffusion would be sufficient to have a sustained effect over the culture period. Levels of passive release are expected to be low due to the tortuous diffusion path through the PEDOT network, as well as the electrostatic interaction between the anionic dopant molecules and the PEDOT backbone. Assuming 100% deposition efficiency, the total amount of DP and VA incorporated in PEDOT/DP and PEDOT/VA coatings was estimated at 0.78 and 0.32 g.cm^{-2} respectively. This corresponds to 1.65 μmol of DP and 2.21

μmol of VA, however the actual amounts incorporated are expected to be considerably lower due to reduced dopant efficiencies. Scaling down to sizes relevant to neural electrodes (50 μm diameter electrode) reduces the potential amount of DP and VA which can be incorporated via a PEDOT coating to 0.032 nmol and 0.043 nmol respectively. It is unlikely that these amounts will be capable of providing a sustained therapeutic effect even under electrically stimulated release.

One promising approach to overcoming the drug-loading and mechanical limitations of bioactive CP coatings is the use of conducting polymer composite materials. Conducting hydrogels (CH) are a class of composites which combine the electrochemical functionality of CPs with the loading capacity and mechanical properties of hydrogels[65,66]. There are numerous reports of CH systems in the literature designed for a variety of applications from stimulating and recording electrodes to electrically controlled drug release devices and biosensors [67–74]. Several different approaches to the fabrication of CHs have been investigated, the most common approach being the electrochemical deposition of CP within a pre-formed hydrogel matrix[67-79]. CHs have mechanical properties akin to that of neural tissue, reducing the strain mismatch at the neural interface which is a contributing factor to the chronic inflammatory response upon implantation[69]. Studies have also shown that CHs are a viable system for the incorporation and controlled release of bioactive factors[68,74,80].

Conclusions

DP and VA were incorporated within PEDOT coatings as bioactive dopants both individually and in a simultaneous co-doped system. A significant reduction in surface area and texture was observed for the bioactive PEDOT coatings. This resulted in a decrease in CSC and an increase in electrochemical impedance when compared to conventional PEDOT/pTS, however, all bioactive films still offer a considerable advantage in charge transfer characteristics compared to bare platinum electrodes. The use of DP and/or VA as dopants did not reduce the electrochemical stability of the PEDOT coatings, but friability remained a problem. Co-doping did reduce friability and improved electroactivity relative to the individual dopants, significantly improving on doping with VA alone. It is concluded that co-doping may provide a mechanism through which bioactive CPs can be developed with stable properties, but it is likely that a conventional dopant, such as pTS may be required as one of the components of such a system.

It was found that both DP and VA retained their bioactivity post-deposition. Furthermore, in an *in vitro* study of inflammation it was determined that one hour of passive diffusion delivered doses sufficient to attenuate a stimulated inflammatory response. However, therapeutic effects were not observed at 14 days in culture with primary astrocyte enriched glial cultures. This was most likely due to limited amounts of available DP and VA, which are expected to be exhausted prior to this time point. Future work will address this limitation

through the incorporation of bioactive dopants within CH bioelectrodes which enable incorporation of greater amounts of biologics within CP based electrode materials.

Acknowledgements

Notes and References

a Graduate School of Biomedical Engineering, University of New South Wales, Sydney 2052, Australia.

1. D. V Bax, R. S. Tipa, A. Kondyurin, M. J. Higgins, K. Tsoutas, A. Gelmi, G. G. Wallace, D. R. McKenzie, A. S. Weiss and M. M. M. Bilek, *Acta Biomater.*, 2012, **8**, 2538–48.
2. D. D. Ateh, H. A. Navsaria and P. Vadgama, *J. R. Soc. Interface*, 2006, **3**, 741–52.
3. L. Cen, K. G. Neoh, Y. Li and E. T. Kang, *Biomacromolecules*, 2004, **5**, 2238–46.
4. J. E. Collazos-Castro, G. R. Hernández-Labrado, J. L. Polo and C. García-Rama, *Biomaterials*, 2013, **34**, 3603–17.
5. J. E. Collazos-Castro, J. L. Polo, G. R. Hernández-Labrado, V. Padial-Cañete and C. García-Rama, *Biomaterials*, 2010, **31**, 9244–55.
6. R. A. Green, N. H. Lovell and L. A. Poole-Warren, *Acta Biomater.*, 2010, **6**, 63–71.
7. R. A. Green, N. H. Lovell, G. G. Wallace and L. A. Poole-Warren, *Biomaterials*, 2008, **29**, 3393–9.
8. R. T. Richardson, B. Thompson, S. Moulton, C. Newbold, M. G. Lum, A. Cameron, G. Wallace, R. Kapsa, G. Clark and S. O'Leary, *Biomaterials*, 2007, **28**, 513–23.
9. J. A. Burdick, M. Ward, E. Liang, M. J. Young and R. Langer, *Biomaterials*, 2006, **27**, 452–9.
10. J. O. Winter, M. Gokhale, R. J. Jensen, S. F. Cogan and J. F. Rizzo, *Mater. Sci. Eng. C. Mater. Biol. Appl.*, 2008, **28**, 448–453.
11. R. Green, PhD Thesis, University of New South Wales, 2009.
12. R. A. Green, N. H. Lovell and L. A. Poole-Warren, *Biomaterials*, 2009, **30**, 3637–44.
13. S. Baek, R. A. Green and L. A. Poole-Warren, *J. Biomed. Mater. Res. A*, 2013.
14. J. H. Collier, J. P. Camp, T. W. Hudson and C. E. Schmidt, *J. Biomed. Mater. Res.*, 2000, **50**, 574–84.
15. S. F. Sorrells and R. M. Sapolsky, *Brain. Behav. Immun.*, 2007, **21**, 259–272.
16. T. Weichhart, O. Brandt, C. Lassnig, M. Müller, W. H. Hörl, G. Stingl and M. D. Säemann, *Immunol. Lett.*, 2010, **129**, 50–52.
17. L. Spataro, J. Dilgen, S. Retterer, A. J. Spence, M. Isaacson, J. N. Turner and W. Shain, *Exp. Neurol.*, 2005, **194**, 289–300.
18. Y. Zhong and R. V. Bellamkonda, *Brain Res.*, 2007, **1148**, 15–27.
19. R. Wadhwa, C. F. Lagenaur and X. T. Cui, *J. Control. Release*, 2006, **110**, 531–41.
20. G. Stevenson, PhD Thesis, University of Wollongong, 2010.
21. G. Stevenson, S. E. Moulton, P. C. Innis and G. G. Wallace, *Synth. Met.*, 2010, **160**, 1107–1114.
22. C.-T. Chiu, Z. Wang, J. G. Hunsberger and D.-M. Chuang, *Pharmacol. Rev.*, 2013, **65**, 105–42.
23. S. Suda, K. Katsura, T. Kanamaru, M. Saito and Y. Katayama, *Eur. J. Pharmacol.*, 2013, **707**, 26–31.
24. K. S. Cho, K. J. Kwon, C. S. Choi, S. J. Jeon, K. C. Kim, J. H. Park, H. M. Ko, S. H. Lee, J. H. Cheong, J. H. Ryu, S. H. Han and C. Y. Shin, *Glia*, 2013, **61**, 694–709.
25. S. Yu, D. Cho, K. Kim, K. Nam, H. Cho and J. Sung, *J Korean Neurosurg Soc.* 2012, **51**, 191–198.
26. J. Biermann, J. Boyle, A. Pielen and W. A. Lagrèze, *Mol. Vis.*, 2011, **17**, 395–403.
27. L. Lv, Y. Sun, X. Han, C. Xu, Y.-P. Tang and Q. Dong, *Brain Res.*, 2011, **1396**, 60–8.
28. Z. Zhang, X. Qin, X. Zhao, N. Tong, Y. Gong, W. Zhang and X. Wu, *Curr. Eye Res.*, 2012, **37**, 429–37.
29. O. Steward, P. Popovich, L. Lv, X. Han, Y. Sun, X. Wang and Q. Dong, *Exp. Neurol.*, 2012, **233**, 783–790.
30. S. Bhandari, N. K. Singha and D. Khastgir, *J. Appl. Polym. Sci.*, 2013, **129**, 1264–1273.
31. A. G. MacDiarmid and A. J. Epstein, *Synth. Met.*, 1995, **69**, 85–92.
32. S. Palaniappan and S. L. Devi, *J. Appl. Polym. Sci.*, 2008, **107**, 1887–1892.
33. D. M. Tigelaar, W. Lee, K. A. Bates, A. Saprigin, V. N. Prigodin, X. Cao, L. A. Nafie, M. S. Platz and A. J. Epstein, *Chem. Mater.*, 2002, **14**, 1430–1438.
34. L. Wei, Q. Chen and Y. Gu, *Synth. Met.*, 2010, **160**, 405–408.
35. S. A. Spanninga, PhD Thesis, The University of Michigan, 2010.
36. S. A. Spanninga, D. C. Martin and Z. Chen, *J. Phys. Chem. C*, 2009, **113**, 5585–5592.
37. ASTM, *D3359 - Standard Test Methods for Measuring Adhesion by Tape Test 1*, 2010.
38. K. D. McCarthy and J. De Vellis, *J. Cell Biol.*, 1980, **85**, 890–902.
39. J. N. Turner, W. Shain, D. H. Szarowski, M. Andersen, S. Martins, M. Isaacson and H. Craighead, *Exp. Neurol.*, 1999, **156**, 33–49.
40. V. S. Polikov, P. a Tresco and W. M. Reichert, *J. Neurosci. Methods*, 2005, **148**, 1–18.
41. M. V Sofroniew and H. V Vinters, *Acta Neuropathol.*, 2010, **119**, 7–35.
42. D. H. Szarowski, M. D. Andersen, S. Retterer, A. J. Spence and M. Isaacson, 2003, **983**, 23–35.
43. R. A. Green, R. T. Hassarati, L. Bouchinet, C. S. Lee, G. L. M. M. Cheong, J. F. Yu, C. W. Dodds, G. J. Suaning, L. A. Poole-Warren and N. H. Lovell, *Biomaterials*, 2012, **33**, 5875–86.
44. B. C. Thompson, S. E. Moulton, R. T. Richardson and G. G. Wallace, *Biomaterials*, 2011, **32**, 3822–31.
45. R. A. Green, S. Baek, N. H. Lovell and L. A. Poole-Warren, in *Nanostructured Conductive Polymers*, John Wiley & Sons, Ltd, 2010, pp. 707–736.
46. B. C. Thompson, S. E. Moulton, J. Ding, R. Richardson, A. Cameron, S. O'Leary, G. G. Wallace and G. M. Clark, *J. Control. Release*, 2006, **116**, 285–94.
47. J.-P. Sylvestre, R. H. Guy and M. B. Delgado-Charro, *Phys. Ther.*, 2008, **88**, 1177–85.
48. J. M. Fonner, L. Forciniti, H. Nguyen, J. D. Byrne, Y.-F. Kou, J. Syeda-Nawaz and C. E. Schmidt, *Biomed. Mater.*, 2008, **3**, 034124.
49. H. Yamato, M. Ohwa and W. Wernet, *J. Electroanal. Chem.*, 1995, **397**, 163–170.
50. H. Randriamahazaka, V. Noël and C. Chevrot, *J. Electroanal. Chem.*, 1999, **472**, 103–111.
51. D. Zhou and E. Greenbaum, in *Implantable Neural Prostheses 2: Techniques and Engineering Approaches*, Springer, 2010, p. 118.
52. S. F. Cogan, *Annu. Rev. Biomed. Eng.*, 2008, **10**, 275–309.
53. W. M. Grill, Indwelling Neural Implants: Strategies for Contending with the In Vivo Environment, W. Reichert, CRC Press 2008.
54. W. M. Grill, S. E. Norman and R. V Bellamkonda, *Annu. Rev. Biomed. Eng.*, 2009, **11**, 1–24.
55. C. O'Neill, *Laryngoscope*, 2000, **110**, 1239.
56. S. Venkatraman, J. Hendricks, Z. A. King, A. J. Sereno, S. Richardson-Burns, D. Martin and J. M. Carmena, *IEEE Trans. Neural Syst. Rehabil. Eng.*, 2011, **19**, 307–16.
57. K. A. Ludwig, J. D. Uram, J. Yang, D. C. Martin and D. R. Kipke, *J. Neural Eng.*, 2006, **3**, 59–70.
58. T. Boretius, M. Schuettler and T. Stieglitz, *Artif. Organs*, 2011, **35**, 245–8.
59. G. R. Hutchison, M. A. Ratner and T. J. Marks, *J. Am. Chem. Soc.*, 2005, **127**, 16866–81.
60. R. J. Kline and M. D. McGehee, *J. Macromol. Sci. Part C Polym. Rev.*, 2006, **46**, 27–45.
61. R. J. Smeyne, G.-S. Peng, G. Li, N.-S. Tzeng, P.-S. Chen, D.-M. Chuang, Y.-D. Hsu, S. Yang and J.-S. Hong, *Mol. Brain Res.*, 2005, **134**, 162–169.
62. J. H. Steer, K. M. Kroeger, L. J. Abraham and D. A. Joyce, *J. Biol. Chem.*, 2000, **275**, 18432–40.
63. A. Xuan, D. Long, J. Li, W. Ji, L. Hong, M. Zhang and W. Zhang, *Life Sci.*, 2012, **90**, 463–468.

64. W. Shain, L. Spataro, J. Dilgen, K. Haverstick, S. Retterer, M. Isaacson, M. Saltzman and J. N. Turner, *IEEE Trans. Neural Syst. Rehabil. Eng.*, 2003, **11**, 186–8.

65. J. Goding, L. Poole-Warren, R. Green and P. Martens, *Ther. Deliv.*, 2012, **3**, 1–7.

66. R. A. Green, S. Baek, L. A. Poole-Warren and P. J. Martens, *Sci. Technol. Adv. Mater.*, 2010, **11**, 014107.

67. L. Pan, G. Yu, D. Zhai, H. R. Lee, W. Zhao, N. Liu, H. Wang, B. C.-K. Tee, Y. Shi, Y. Cui and Z. Bao, *Proc. Natl. Acad. Sci. U. S. A.*, 2012, **109**, 9287–92.

68. L. M. Lira and S. I. Córdoba de Torresi, *Electrochem. commun.*, 2005, **7**, 717–723.

69. R. A. Green, R. T. Hassarati, J. A. Goding, S. Baek, N. H. Lovell, P. J. Martens and L. A. Poole-Warren, *Macromol. Biosci.*, 2012, **12**, 494–501.

70. B. C. Kim, G. M. Spinks, G. G. Wallace and R. John, 2000, **41**, 1783–1790.

71. S. Sekine, Y. Ido, T. Miyake, K. Nagamine and M. Nishizawa, *J. Am. Chem. Soc.*, 2010, **132**, 13174–5.

72. G. L. Mario Cheong, K. S. Lim, A. Jakubowicz, P. J. Martens, L. A. Poole-Warren and R. A. Green, *Acta Biomater.*, 2014, **10**, 1216–26.

73. S. K. Siddhanta and R. Gangopadhyay, *Polymer (Guildf).*, 2005, **46**, 2993–3000.

74. R. C. Barthus, L. M. Lira and S. I. C. De Torresi, 2008, **19**, 630–636.

75. G. Justin and A. Guiseppi-Elie, *Biomacromolecules*, 2009, **10**, 2539–49.

76. Y. Xia and H. Zhu, *Soft Matter*, 2011, **7**, 9388.

77. T. Dai, X. Qing, H. Zhou, C. Shen, J. Wang and Y. Lu, *Synth. Met.*, 2010, **160**, 791–796.

78. B. Guo, A. Finne-Wistrand and A.-C. Albertsson, *Chem. Mater.*, 2011, **23**, 1254–1262.

79. T. Dai, X. Qing, Y. Lu and Y. Xia, *Polymer (Guildf).*, 2009, **50**, 5236–5241.

80. J. Lin, Q. Tang, J. Wu and Q. Li, *J. Applied Poly. Sci.*, 2010, **116**, 1376–1383.

81. J. Xu, G. Shi, F. Chen, X. Hong, *Chin. J. Poly. Sci.*, 2002, **20**, 425-430

Journal of Materials Chemistry B Accepted Manuscript
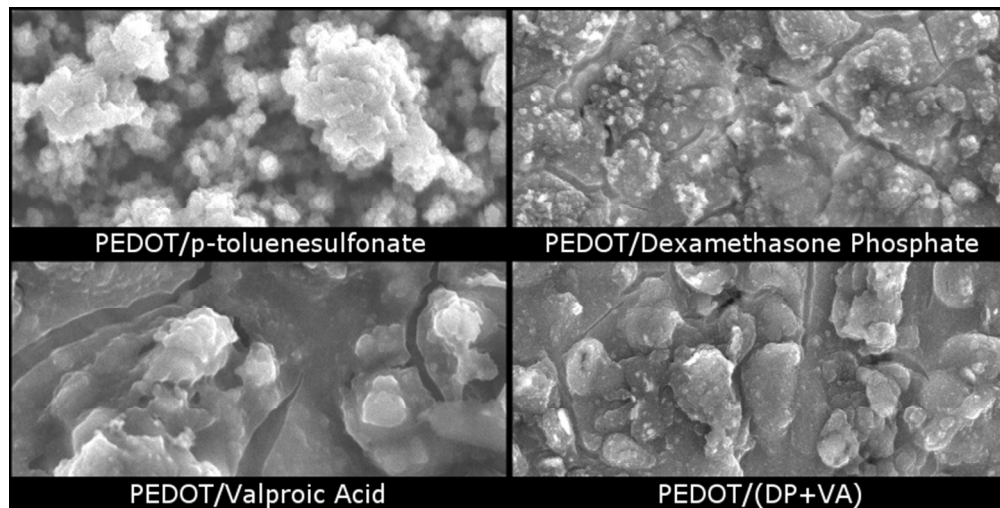
Scanning electron microscope image of surface morphology of conducting polymer PEDOT doped with bioactive molecules.
79x39mm (256 x 256 DPI)